Monte Carlo simulation of glandular dose in a dedicated breast CT system*

TANG Xiao(唐晓)[1,2,3;1)] ZHAO Wei(赵维)[1,2,3] WANG Yan-Fang(王燕芳)[1,2] SHU Hang(舒航)[1,2]
SUN Cui-Li(孙翠丽)[1,2] WEI Cun-Feng(魏存峰)[1,2] CAO Da-Quan(曹大泉)[1,2,3]
QUE Jie-Min(阙介民)[1,2] SHI Rong-Jian(史戎坚)[1,2] WEI Long(魏龙)[1,2]

[1] Key Laboratory of Nuclear Analytical Techniques, Institute of High Energy Physics, Chinese Academy of Sciences, Beijing 100049, China
[2] Beijing Engineering Research Center of Radiographic Techniques and Equipment, Beijing 100049, China
[3] Graduate University of Chinese Academy of Sciences, Beijing 100049, China

Abstract: A dedicated breast CT system (DBCT) is a new method for breast cancer detection proposed in recent years. In this paper, the glandular dose in the DBCT is simulated using the Monte Carlo method. The phantom shape is half ellipsoid, and a series of phantoms with different sizes, shapes and compositions were constructed. In order to optimize the spectra, monoenergy X-ray beams of 5–80 keV were used in simulation. The dose distribution of a breast phantom was studied: a higher energy beam generated more uniform distribution, and the outer parts got more dose than the inner parts. For polyenergtic spectra, four spectra of Al filters with different thicknesses were simulated, and the polyenergtic glandular dose was calculated as a spectral weighted combination of the monoenergetic dose.

Key words: dedicated breast CT, Monte Carlo simulation, glandular dose

PACS: 81.70.Tx, 02.70.Uu, 87.53.Bn **DOI:** 10.1088/1674-1137/36/7/019

1 Introduction

Breast cancer is the most frequently diagnosed cancer in women, and ranks second as a cause of cancer death in women (after lung cancer). Mammography can detect breast cancer at an early stage, when treatment is more effective and a cure is more likely. It provides projections in which calcifications and small tumors can be seen. But as a two dimensional imaging method, overlaying in projection direction is not avoidable. To solve this theoretical problem, many groups are investigating the dedicated breast CT system [1]. The DBCT images the breast in hundreds of directions in a circle, and provides three dimensional images of the breast in which tumors can be distinguished more easily. However, this system may cause concern if an incorrect dose, despite the better image, results in a rise in the risk of radiation carcinogenesis [2]. Thus the accurate measurement of the mean glandular dose is a critical issue to evaluate the system.

There are two main ways to measure the dose absorbed in breast tissue through Monte Carlo simulations and experiments. Through Monte Carlo simulations, the factors affecting the result can be calculated separately. Since the spectra, the breast size, material and geometry all affect dose, it is meaningful to investigate their influence respectively. Also, this method is fast and easy, and has been a useful method for breast dosimetry in mammography [3]. Several groups have investigated the dose of DBCT in this way [4, 5]. Boone et al introduced and provided a set of DgNCT [6], which is a normalized glandular dose coefficient for CT. The average glandular dose for one CT scan can be obtained by multiplying the DgNCT specified from the scan parameter to the air kerma at the isocenter. They simulated the glandular dose using monoenergy X-ray beams, which makes clear the dose dependency of the beam energy. But their phantom shape is of a cylinder, which varies from

Received 22 October 2011, Revised 17 November 2011
* Supported by Knowledge Innovation Project of Chinese Academy of Sciences (KJCX2-EW-N06)
1) E-mail: tangxiao@ihep.ac.cn

breast shapes. On the other hand, experiments have also been carried out to verify the results of simulations. Russo et al examined the dose distribution [7] in a breast shaped polymethyl methacrylate (PMMA) phantom by putting several thermoluminescent dosimeters (TLD) into different positions, and the dose distribution of the phantom was studied.

In this paper, we use the Monte Carlo method to simulate the glandular dose in the DBCT system, and change the phantom shape from a cylinder which is commonly used into a half ellipsoid which resembles a breast more. Reported by Yi et al., "The results show that dose estimates with ellipsoidal phantoms were close to those with the structured breast models. The dose estimates with the cylindrical phantoms, on the other hand, were found to be consistently lower." [5] Mostly a 5–80 keV monoenergy X-ray beam is used, and the dose distribution and the influence of breast size, shape and composition are shown in this work. Not much work has been done with polyenergy beams, as the optimization of the spectra should be done with the consideration of image quality.

2 Material and methods

2.1 Monte Carlo platform

Geant4 is a toolkit for the simulation of the passage of particles through matter, which is a well established and validated code for radiation transport. The spectra were simulated using Geant 4. GATE (Geant 4 application for tomographic emission) was used in the monoenergetic CT dose simulations, which is a dedicated simulation platform for emission tomography based on Geant 4 [8]. The initial uses were mainly in single photon emission computed tomography (SPECT) and positron emission tomography (PET), but a new version, GATE V6, has enabled modeling of X-ray computed tomography and radiation therapy experiments. Radiation therapy processes include specialized dose application. The physical process involves photoelectric, Raleigh, and Compton scattering. Photons penetrate the digital phantom And interact with it by the probability at each energy. The energy deposit is recorded and used in the calculation of dose.

2.2 Phantom and geometry

Breast tissue is constituted of glandular and adipose tissue with various distributions, and is covered by 3–5 mm skin. Only the glandular tissues are at high risk, and Hammerstein et al. suggested that the mean dose to the glandular tissues within the breast should be the concerned quantity [9]. To calculate the glandular dose, the ideal method is first to construct a structured digital phantom, then simulate the exposure, and then average the dose of all the glandular voxels. But this procedure is time consuming, and compared by Yi et al. the values for structured models have little difference with those for homogeneous models [5]. So in our simulation a homogeneous breast tissue model with different mass proportions were used, and the outermost part of 4 mm was skin.

The density and the elemental composition of tissues are required to construct material. Data of glandular, adipose and skin tissues are acquired from the report by Hammerstein et al. [9]; the elemental compositions of glandular adipose tissues are weighted by the sum of their mass proportion, and the densities are calculated by

$$\rho_{\rm b} = \frac{\rho_{\rm a}\rho_{\rm g}}{f_{\rm g}\rho_{\rm a} + f_{\rm a}\rho_{\rm g}},$$

where ρ stands for the density, f stands for the mass fraction, and subscript b refers to the breast tissue, a refers to the adipose, and g refers to the glandular. Phantom shape is constructed as half ellipsoid, instead of the cylinder shape often used in simulations. The geometry of the simulation is shown in Fig. 1.

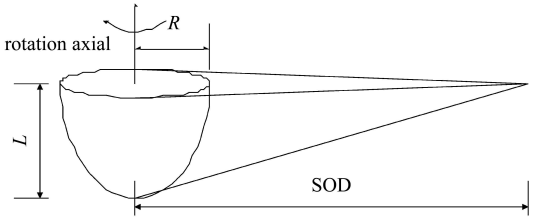

Fig. 1. The diagram shows the geometry used for Monte Carlo simulations. R=radius of the cross-section circle, L= the height of half ellipsoid, SOD=source-to-object distance.

Table 1. The simulation parameters.

source angle	13.8° (bottom half)
number of photons	10^7
rotation angle	360°
SOD	60 cm

Photons produced by the source emitted in the direction of the half cone beam. The cone angle is 13.8°, and only in the bottom half of the cone. The source is defined as a 0.5 mm square plane. 10 million primary photons were run in one simulation. To rotate the phantom, each run was split into 360 time slices, phantom rotated by 1° in each time slice, and the primary photons emitted evenly in each time slice.

The simulation parameters are illustrated in Table 1, and a projection image is shown in Fig. 2.

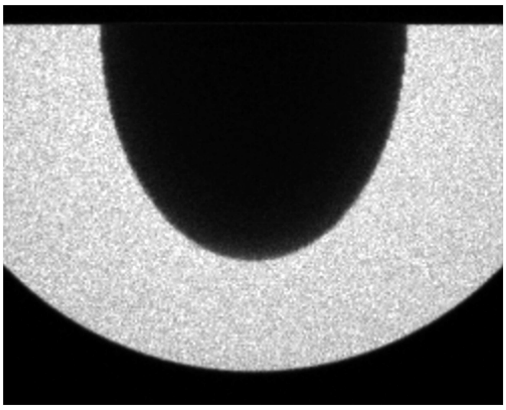

Fig. 2. Projection of an R=6.5 cm, L=10 cm phantom. SOD=60 cm, detector-to-object distance is 10 cm, with the upper edge of the detector 10 cm higher than the horizontal plan.

2.3 Calculation of the glandular dose

With the combination of target material, tube voltage and filter alteration, spectra can be various. For the sake of generality, monoenergetic beams were used in each run, and 5–80 keV photon beams had been simulated by a 1 keV step. Polyenergetic dose within that energy domain can be obtained as a spectral weighted combination of the monoenergetic dose. Let $\overline{D}(E)$ be the average dose of the monoenergetic beam with photon energy E, divided by the primary photon number in unit area, let Φ(E) be the spectra in photon number per unit area, and let $G(E)$ be the component correction coefficient, then the polyenergetic glandular dose D_{g} was calculated by

$$D_{\mathrm{g}} = \sum_{E=E_{\min}}^{E_{\max}} \overline{D}(E)\Phi(E)G(E).$$

In each monoenergetic run, a dose record actor was attached to the phantom, and rotated with the phantom. The dose actor was set as a 3D array of 1 mm× 1 mm×1 mm voxel size, and $\overline{D}(E)$ was the average of the voxel dose within the breast tissue volume

$$\overline{D} = \frac{1}{N}\sum_{i=1}^{N} D(i),$$

where N is the total number of breast tissue voxels, and $D(i)$ is the dose for the ith voxel.

$G(E)$ is multiplied as $\overline{D}(E)$, an average dose of homogenous breast tissue constituted by glandular and adipose tissues, and the glandular portion should be extracted from that. The expression of $G(E)$ is

$$G(E) = \frac{f_{\mathrm{g}}\left(\frac{\mu_{\mathrm{en}}(E)}{\rho}\right)_{\mathrm{g}}}{\left[f_{\mathrm{g}}\left(\frac{\mu_{\mathrm{en}}(E)}{\rho}\right)_{\mathrm{g}} + (1-f_{\mathrm{g}})\left(\frac{\mu_{\mathrm{en}}(E)}{\rho}\right)_{\mathrm{a}}\right]} \cdot \frac{1}{f_{\mathrm{g}}},$$

where $(\mu_{\mathrm{en}}(E)/\rho)_{\mathrm{g}}$ and $(\mu_{\mathrm{en}}(E)/\rho)_{\mathrm{a}}$ stand for the mass energy absorption coefficients for glandular and adipose tissues, and f_{g} stands for the mass fraction of glandular tissues. As dose is the deposited energy divided by mass, the front fraction is for the deposited energy, and the latter $1/f_{\mathrm{g}}$ is for the mass.

The spectra $\Phi(E)$ were simulated in Geant4 on the other hand. 10^8 monoenergetic electrons were ejected to the tungsten anode to generate X-ray photons, and the photons passing through a 50 μm beryllium window were recorded by an ideal photon counter detector. A flow chart of the whole process was illustrated in Fig. 3.

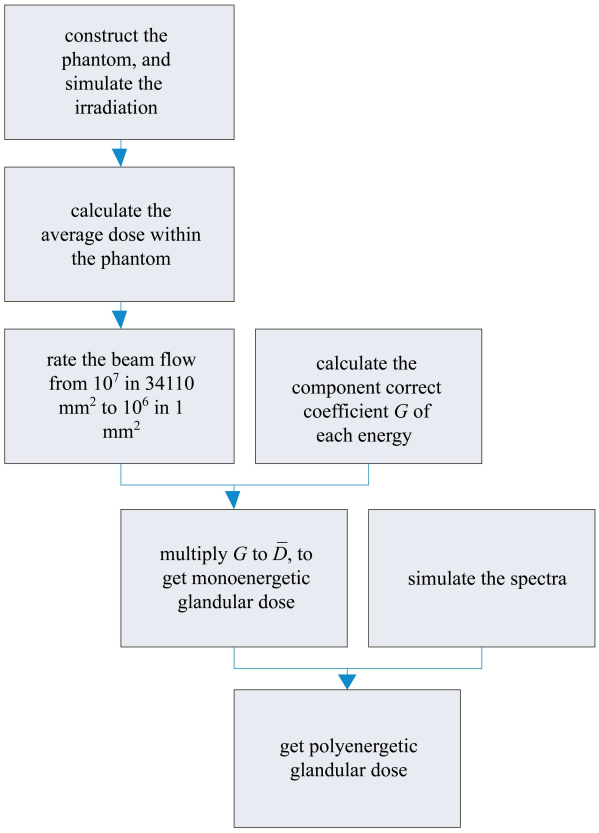

Fig. 3. Flow chart of the glandular dose simulation in DBCT.

3 Results

3.1 Dose deposition

As the X-ray penetrates the phantom, the energy deposition is high on the surface, and becomes less in

the deeper area. For the sake of rotation, the dose deposition is of axial symmetry. The difference along the radius is more evident with a lower energy beam, because a lower energy beam has worse penetrability than a higher energy beam. Fig. 4 shows the coronal cross sections of dose deposition, while Fig. 5 shows the sagittal cross sections of that. Both of them are in the same position of a 13 cm diameter 10 cm height 50% glandular phantom, and irradiated by 20 keV and 60 keV photon beams respectively.

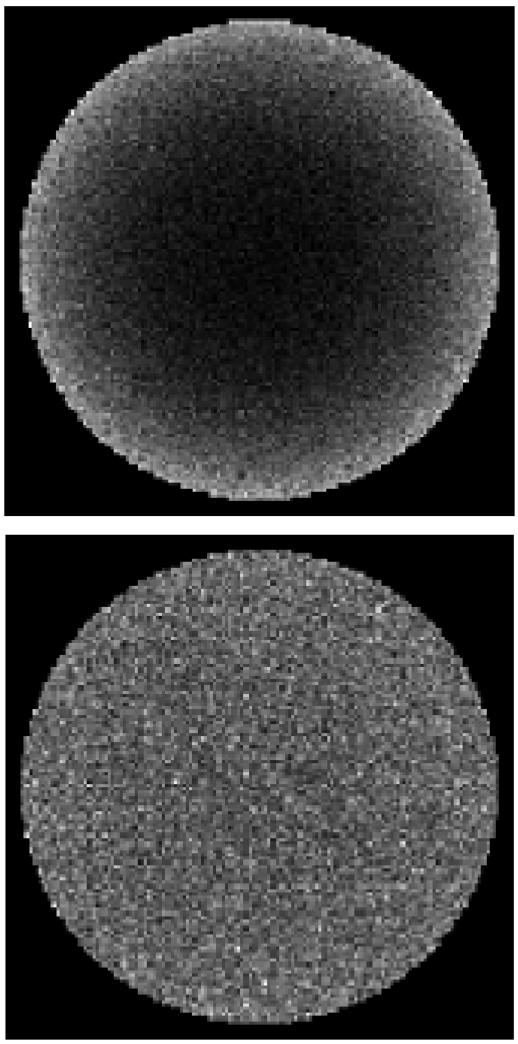

Fig. 4. The coronal cross sections of dose deposition. top: the 20 keV monoenergy beam; down: the 60 keV monoenergy beam.

3.2 Influence of breast size and shape

Compressed breasts are categorized explicitly by thickness. For uncompressed breasts, we simply categorize the breast size into S, M, and L. For breasts with the same diameter, the breast shape differs with each patient, and mostly affects the breast length. Size M was taken as an example, and shape MM, MS, ML were checked. All these phantoms are 50% glandular. The radius and length of phantoms used are shown in Table 2.

Table 2. The radius and length of phantoms for breast size and shape simulation.

	breast size			breast shape		
	S	M	L	MS	MM	ML
R/cm	5.5	6.5	7.5	6.5	6.5	6.5
L/cm	8	10	12	8	10	12

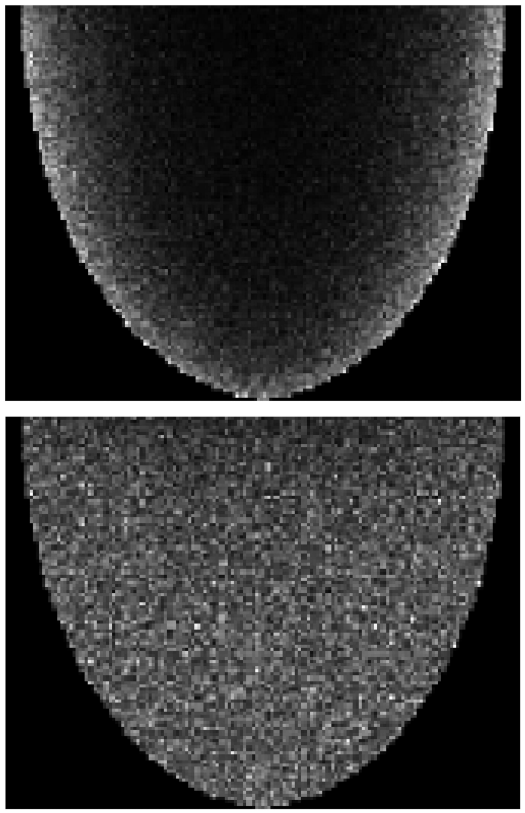

Fig. 5. The sagittal cross sections of dose deposition. top: the 20 keV monoenergy beam; down: the 60 keV monoenergy beam.

The Monte Carlo results for monoenergetic glandular dose of three size breasts are illustrated in Fig. 6(a). Monoenergetic glandular dose (MGD) is very low under 7 keV, and almost no X-ray can penetrate the skin layer. The X-ray energy between 20 and 30 keV generates the most energy deposition within breast tissue under the same beam fluence. The small phantom got the most MGD while the large phantom got the least MGD under the same beam energy. Fig. 6(b) shows how the breast length influences the dose for the same radius breasts. It is indicated that shorter breasts got less MGD than longer breasts. But its influence is much less than the breast size. The MGD variance is mainly dependent on the breast radius.

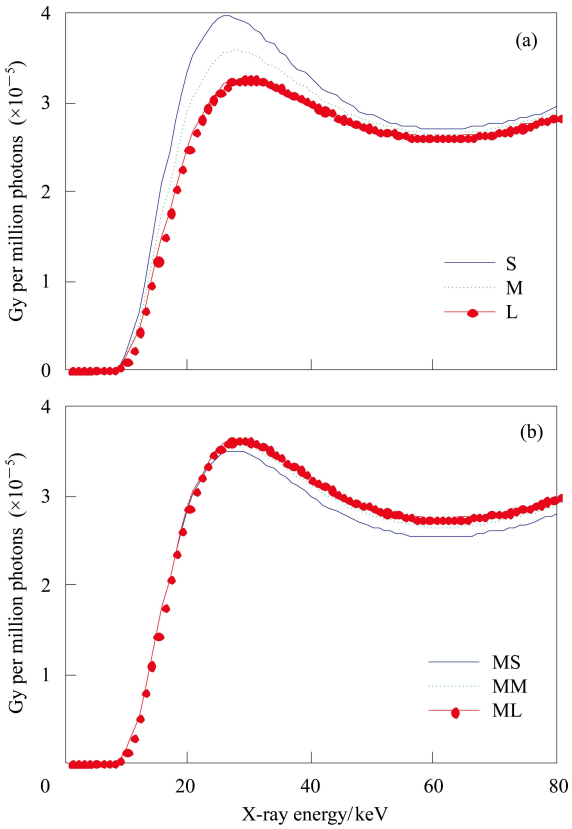

Fig. 6. The graphs show the monoenergetic glandular dose as a function of incident X-ray energy for (a) three different breast sizes of S, M, and L; (b) three different breast shapes of MS, MM, and ML.

3.3 Influence of composition

Figure 7 demonstrates the MGD of the M size phantom for three different compositions: 0% glandular, 50% glandular and 100% glandular. With X-ray energy under 50 keV, the MGD of the low glandularity breast tissue is much higher. With X-ray energy beyond 50 keV, the MGD of different breast compositions are close and the high glandularity breast tissue data is a little higher.

3.4 Spectra

Figure 8 shows four spectra simulated with 2 mm, 4 mm, 6 mm, and 8 mm Al filters, and a tube voltage of 70 kV. The electron beams are all converted to 1 mAs, and the beam flux gets lower with a thicker filter, and the beam effective energy gets higher.

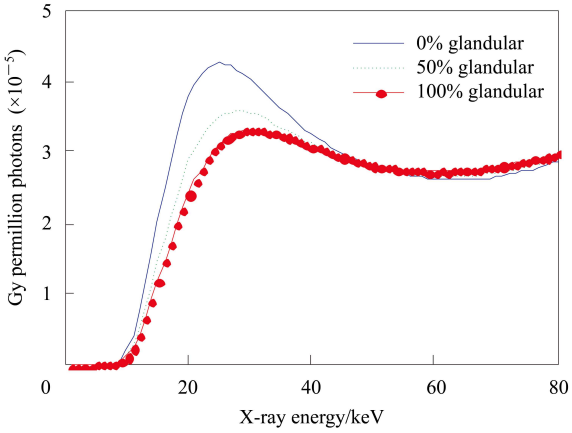

Fig. 7. The graph shows a monoenergetic glandular dose as a function of incident X-ray energy for 0%, 50%, and 100% glandular tissue.

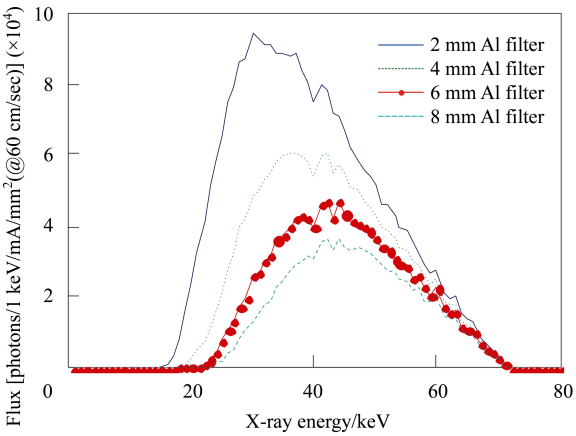

Fig. 8. The X-ray spectra $\Phi(E)$ of the W anode simulated with same 70 kV voltage and Al filters of different thicknesses.

Using these spectra and the formulas in 2.3, the average glandular dose of four spectra and three breast sizes are computed, all the phantoms are 50% glandular.

Table 3. The radius and length of phantoms for breast size and shape simulation.

average glandular dose/(Gy/mAs)		filters			
		2 mmAl	4 mmAl	6 mmAl	8 mmAl
breast sizes	11 cm/8 cm	9.17E-05	5.75E-05	4.00E-05	2.95E-05
	13 cm/10 cm	8.60E-05	5.46E-05	3.82E-05	2.83E-05
	15 cm/13 cm	8.10E-05	5.20E-05	3.66E-05	2.73E-05

The polyenergetic average glandular dose result is consistent with the monoenergetic glandular dose. With a specific spectrum, the average glandular dose can be calculated in this way, and then multiplied by mAs, the total average glandular dose is determined. The optimal spectra and the mAs needed should be evaluated in cooperation with the image quality.

4 Discussion and conclusion

In this work, we showed a Monte Carlo simulation result about dose in a cone-beam breast CT system. A set of breast phantoms was constructed, with different breast sizes, shapes and compositions, and 5–80 keV monoenergetic X-ray beams were used to check their dose respectively. From coronal and sagittal cross sections of dose distribution, it is revealed that positions closer to the surface got a higher dose, and a lower energy beam generated higher nonuniformity. For different size phantoms, the results show that under the same beam conditions, a bigger breast got a lower glandular dose. For different composition phantoms, low glandularity breasts got a higher glandular dose with a monoenergetic X-ray beam under 50 keV.

Derivation of the polyenergetic average glandular dose is described in this paper. In future studies, we shall work on the optimization of spectra in cooperation with the image quality. The penetrability should suit the breast density properly, and the dose efficiency be maximized.

References

1 Schmidt T G. Current Medical Imaging Reviews, 2010, **6**(2): 61–71
2 Boone J M, Nelson T R, Lindfors K K et al. Radiology, 2001, **221**(3): 657–667
3 Boone J M. Radiology, 1999, **213**(1): 23–37
4 Thacker S C, Glick S J. Physics in Medicine and Biology, 2004, **49**(24): 5433–5444
5 YI Y, LAI C J, HAN T et al. Medical Physics, 2011, **38**(2): 589–597
6 Boone J M, Shah N, Nelson T R. Medical Physics, 2004, **31**(2): 226–235
7 Russo P, Lauria A, Mettivier G et al. Ieee Transactions on Nuclear Science, 2010, **57**(1): 366–374
8 Jan S, Benoit D, Becheva E et al. Physics in Medicine and Biology, 2011, **56**(4): 881–901
9 Hammerstein G R, Miller D W, White D R et al. Radiology, 1979, **130**(2): 485–491